PCCP

Accepted Manuscript

ROYAL SOCIETY OF CHEMISTRY

www.rsc.org/pccp

Exfoliating biocompatible ferromagnetic Cr- trihalide monolayers

Junyi Liu,[a] Qiang Sun,[a,b,c,*] Yoshiyuki Kawazoe,[d] Puru Jena[c]

[a] Department of Materials Science and Engineering, Peking University, Beijing 100871, China

[b] Center for Applied Physics and Technology, Peking University, Beijing 100871, China

[c] Department of Physics, Virginia Commonwealth University, Richmond, VA 23284, USA

[d] New Industry Creation Hatchery Center, Tohoku University, Sendai, 980-8577, Japan

*sunqiang@pku.edu.cn

Abstract

In addition to spintronics another motivation for exploring ferromagnetic two-dimensional materials is for biomedical applications such as magnetic labeling and hyperthermia treatment of tumors. Unfortunately, the widely studied Mn-containing monolayer is not biocompatible, although it is ferromagnetic. Here using first principles calculations combined with Monte Carlo simulations based on Ising model, we systematically study a class of 2D ferromagnetic monolayers CrX_3 (X= Cl, Br, I). The feasibility of exfoliation from their layered bulk phase is confirmed by the small cleavage energy and high in-plane stiffness. Spin-polarized calculations, combined with self consistently determined Hubbard U that accounts for strong correlation energy, demonstrate that CrX_3 (X=Cl, Br, I) monolayers are ferromagnetic and Cr is trivalent and carries a magnetic moment of $3\mu_B$, the resulting Cr^{3+} ions are biocompatible. The corresponding Curie temperatures for $CrCl_3$ $CrBr_3$ CrI_3 are found to be 66, 86, and 107 K, respectively, which can be increased to 323, 314, and 293 K by hole doping. The biocompatibility and ferromagnetism render these Cr-containing trihalide monolayers unique for applications.

Introduction

The exceptional electrical, thermal and mechanical properties of graphene[1, 2] have motivated scientists to explore other two-dimensional materials, especially those that are biocompatible and exhibit strong ferromagnetism. For example, conventional methods such as surgery and chemotherapy for treating malignant tumors are invasive with adverse side effects. An ideal way to treat cancer is to selectively destroy the cancer cells without damaging normal tissue. Biocompatible ferromagnetic 2D materials with large surface area hold some promise in this area. Magnetically directed drug delivery, combined with hyperthermia induced by near infrared light or an alternating magnetic field, would destroy the tumor cells effectively. One of the key requirements for such applications is for the materials to be ferromagnetic and biocompatible. Unfortunately, graphene and its analog such as BN sheet, silicene, MoS_2, WS_2[3-5] are intrinsically nonmagnetic in their pristine form. While it is possible to introduce magnetism in these systems by doping[6, 7], the distribution of doped magnetic atoms in is highly sensitive to the synthesis process and ambient conditions, low solubility and surface clustering[8-10] being among the major problems. For example, the binding energy of a Cr atom supported on graphene is about 0.5 eV and the migration energy barrier is only 0.02 eV.[11] This suggests that metal atoms on graphene quickly migrate across the lattice and bind together forming clusters. The question then arises: Can one find a pristine 2D monolayer that contains transition metal (TM) ions in its intrinsic backbone and is ferromagnetic and biocompatible? It has been found that many Mn-containing monolayers such as MnO_2, Pc-Mn, MnX_2 (X=S, Se), and Mn-CN[12-15] are ferromagnetic with high Curie temperatures. However, Mn^{2+} and Mn^{3+} are neurotoxic[16] and may enter the brain by crossing the blood-brain barrier and cause permanent neurological damage.

In this paper we explored the possibility that Cr monolayers may provide the answer. Cr with an electronic configuration of $3d^5 4s^1$ possesses the largest atomic magnetic moment, namely $6\mu_B$, of all elements in the 3d transition metal series. Furthermore, the trivalent chromium (Cr^{3+}) is biocompatible and is widely found in

food and supplements.[17] Although Zhang et al. computationally designed a 2D CrN sheet[18] and found this sheet to have strong ferromagnetism, no evidence was provided to show that it can be synthesized. Note that no such layered materials are known to exist in the nature.

Here, we show that chromium trihalides, CrX_3 (X = Cl, Br, I), are good candidates. The underlying reasons are the following: (1) Just like MoS_2, the chromium trihalides are another class of van der Waals (vdW) bonded, layered semiconductors.[19-21] Thus, it is possible to produce monolayers by exfoliation. (2) The exfoliated CrX_3 monolayers would ensure Cr to be trivalent and sandwiched Cr^{3+} ions are biocamptible. (3) In the layered bulk phase of CrX_3 (X = Cl, Br, I),[22] the in-plane magnetic coupling is ferromagnetic, which can be expected to remain ferromagnetic when exfoliated into monolayers. We confirm these expectations through detailed first-principles calculations.

Using density functional theory (DFT) based calculations combined with Monte Carlo simulations based on the Ising model, we have systematically studied the electronic structure, stability, and magnetic properties of CrX_3 (X = Cl, Br, I). We find the cleave energy to be smaller than that of graphite, indicating that it can be easily exfoliated. Moreover, 2D CrX_3 (X = Cl, Br, I) monolayer has a relative high in-plane stiffness so that it can maintain free-standing planarity. Optimized 2D CrX_3 (X = Cl, Br, I) monolayer is found to be a ferromagnetic semiconductor. The Curie temperature estimated by Monte Carlo simulations based on the Ising model is 66, 86, 107 K, for $CrCl_3$, $CrBr_3$, and CrI_3, respectively, which can be significantly increased by hole doping to 323, 314, 293 K.

Method

Our first principles calculations are based on spin-polarized density functional theory with Perdew−Burke−Ernzerhof form for generalized gradient approximation (GGA)[23] to exchange-correlation potential as implemented in the Vienna ab initio Simulation Package (VASP).[24] Projector Augmented Wave (PAW)[25] method is used to

treat interactions between ion cores and valance electrons with 400 eV kinetic energy cutoff of plane waves. For the 2D monolayer, a unit cell with periodic boundary conditions is adopted to simulate the infinite x-y plane, and a vacuum of 15 Å along z axis is applied to avoid interaction between two neighboring images. The Monkhorst-Pack special k-point scheme with 9x9x1, and 5x5x1 grid meshes are used to represent the reciprocal space of unit cell and 2x2 supercell, respectively. For the bulk crystal, the Grimme's DFT-D2 dispersion correction[26] is applied to account for the long-range van der Waals interactions between different layers. The geometric structure is relaxed using the conjugated gradient method without any symmetry constraint until the Hellmann-Feynman force on each atom is smaller than 0.01 eV/Å. Total energy is converged to 10^{-4} eV.

It is well known that GGA cannot properly describe strongly correlated systems containing partially filled *d* subshells. Moreover, the previous theoretical study of bulk CrX_3 (X=Cl, Br, I) crystals[19] show that one can get ferromagnetic ordering in agreement with experiment results for $CrBr_3$ and CrI_3 via GGA method, but the antiferromagnetic state of $CrCl_3$ can only be reproduced by introducing on-site electron–electron repulsion. Thus, it is necessary to take on-site Coulomb repulsion of Cr 3d electrons into account using the GGA+U method for the energy comparisons between ferromagnetic and antiferromagnetic states in the same calculation level. Usually, the value of U is taken as a semi-empirical parameter and is obtained by comparing different calculated physical properties with experimental results. However, for the CrX_3 (X= Cl, Br, I) monolayers, there are no direct experimental results available. Hence, we calculate U self-consistently from first-principles by using the linear response approach proposed by Cococcioni and Gironcoli,[27] in which U is determined by the difference between the screened and bare second derivative of the energy with respect to localized state occupations n^I at site *I*. This can be written as

$$U = \frac{\partial^2 E[\{n^I\}]}{\partial (n^I)^2} - \frac{\partial^2 E_0[\{n^I\}]}{\partial (n^I)^2}$$

Applying localized potential shifts to the *d* levels of the Cr atoms to excite charge

fluctuation on their orbitals, and solving the Kohn-Sham equations self-consistently, we can get an occupation-dependent energy functional

$$E[\{n^I\}] = \min_{\alpha_I}\{E[\{\alpha_I\}] - \sum_I \alpha_I n^I\}$$

And

$$\frac{\partial E[\{n^I\}]}{\partial n^I} = -\alpha_I(\{n^I\})$$

$$\frac{\partial^2 E[\{n^I\}]}{\partial (n^I)^2} = -\frac{\partial \alpha_I(\{n^I\})}{\partial n^I}$$

Using α_I as the perturbation parameter, the effective interaction parameter U of site I can then be obtained as,

$$U = \frac{\partial \alpha_{I,0}}{\partial n_I} - \frac{\partial \alpha_I}{\partial n_I} = [\chi_0^{-1} - \chi^{-1}]^I$$

In the above derivation U is calculated from the GGA ground state; it should be consistently obtained from the GGA+U ground state itself, which may be especially relevant when GGA and GGA+U differ qualitatively (metal versus insulator in the solid state). To solve this problem, Kulik et al[28] have identified that the electronic terms in the GGA+U functional have quadratic dependence on the occupations:

$$E_{quad} = \frac{U_{scf}}{2}\sum_I [\sum_i n_i^I (\sum_j n_j^I - 1)] + \frac{U_{in}}{2}\sum_I \sum_i n_i^I (1 - n_i^I)$$

where U_{scf} represents the effective on-site electron-electron interaction already present in the GGA energy functional for the GGA+U ground state when U is chosen to be U_{in}. The second derivative of E_{quad} with respect to n_i^I also corresponds to the U_{out} obtained from linear-response:

$$U_{out} = \frac{d^2 E_{quad}}{d(n_T^I)^2} = U_{scf} - \frac{U_{in}}{m}$$

Thus, U_{out} is linear in U_{in} for the relevant range of $U_{in} \sim U_{scf}$. From a few linear-response calculations for different U_{in} ground states, we can extract the U_{scf} that should be used for the 2D sheets. The self-consistent determination of U is performed with the

quantum espresso (QE) code[29] using GGA (PBE) exchange-correlation functional and PAW pseudopotentials. The wave-function and electronic density cut-off energies are set as 35 Ry and 300 Ry, respectively, which are tested to be large enough for desired accuracy.

Results and Discussion

1. Cleavage energy

First, we examine the feasibility of exfoliating a monolayer from the bulk CrX_3 (X= Cl, Br, I) by calculating the cleavage energy. The bulk CrX_3 (X= Cl, Br, I) has two kinds of stacking sequence,[30] as shown in the Figure 1, one is rhombohedral BiI_3 structure type (space group $R\bar{3}$) at low temperature and the other is monoclinic $AlCl_3$ structure type (space group C2/m) at high temperature. Here, cleavage energies of both structure types are calculated using the following procedure: introducing a fracture in the bulk and then gradually increasing the separation between the two fractured parts and measuring the variation of total energy. The total energy is seen to increase with separation d_t at first, and then slowly converges to the ideal cleavage cohesion energy. For the rhombohedral (monoclinic) structure, the calculated cleavage energy is 0.10 (0.13), 0.14 (0.19), and 0.16 (0.25) J/m^2 for $CrCl_3$, $CrBr_3$ and CrI_3, respectively. Our results for CrI_3 agrees well with the previous theoretical study[30] performed using optB86b exchange functional to consider the long-ranged van der Waals forces. This indicates the reliability of our calculations. All the above cleavage energies are smaller than that of graphite (~0.36 J/m^2), demonstrating that the 2D CrX_3 (X= Cl, Br, I) monolayers can be cleaved easily from their layered bulk phases.

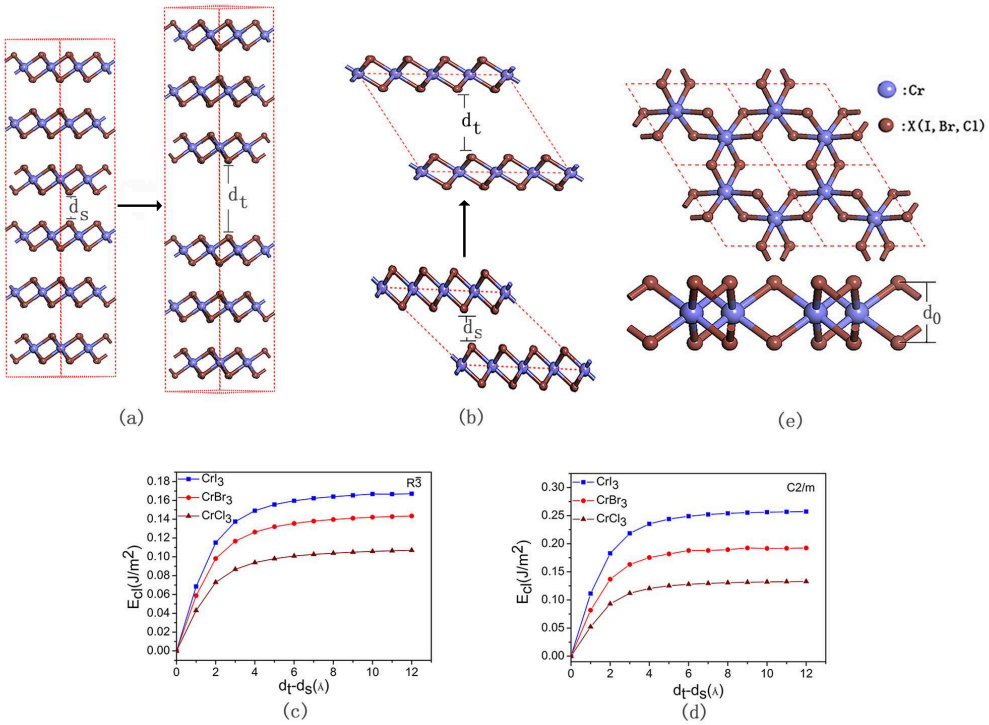

Figure 1 Bulk CrX_3 (X= Cl, Br, I) with (a) rhombohedral and (b) monoclinic structure seen from side view with the corresponding fracture used to simulate the exfoliation procedure; Cleavage energy E_{cl} for the (c) rhombohedral and (d) monoclinic structure as a function of the separation between two fractured parts; (e) Top and side views of the CrX_3 (X= Cl, Br, I) monolayer, d_0 is the vertical distance between two halide planes.

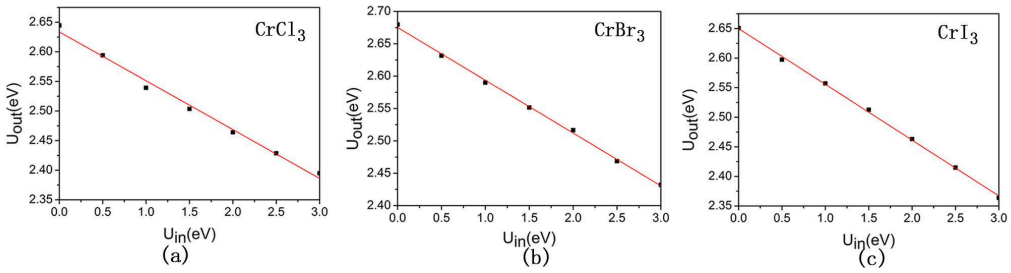

Figure 2 Linear response U_{out} calculated from the GGA+U_{in} ground state of (a) $CrCl_3$, (b) $CrBr_3$, and (c) CrI_3 monolayer.

2. Effective onsite coulomb interaction (U)

Now, we focus our studies on CrX_3 (X= Cl, Br, I) monolayers. In figure 2, we plot U_{out} as a function of U_{in}, which shows a good linear relationship. Hence, the extrapolated U for $CrCl_3$, $CrBr_3$, and CrI_3 are 2.63, 2.68 and 2.65 eV, respectively. These values are close to each other as Cr has similar bonding environment in all the three compounds. Using the self-consistent value of U, we fully relax the lattices and atomic positions of CrX_3 (X=Cl, Br, I) monolayer, and calculate the geometric parameters. These are listed in the Table 1. We find that the lattice constant, Cr-halide bond length, and d_0 (vertical distance between two halide planes) increase from the $CrCl_3$ to the CrI_3, which is consistent with the increasing atomic radius from chlorine to iodine. Moreover, the calculated Cr-halide bond length of CrX_3 (X= Cl, Br, I) monolayer is similar to that of bulk crystal reported in previous experimental and theoretical works,[19, 30] showing that our calculation with GGA+U method is reasonable.

Table 1 The optimized geometrical parameters: Lattice parameter (a_0); Cr–X bond length (d_{Cr-X}); Interlayer distance between two halide planes (d_0), and the mass density (ρ) of 2D CrX_3.

Compound	a_0 (Å)	d_{Cr-X} (Å)	d_0 (Å)	$\rho(10^{-6}$ kg $m^{-2})$
$CrCl_3$	6.108	2.380	2.698	3.2
$CrBr_3$	6.496	2.545	2.909	5.3
CrI_3	7.079	2.771	3.174	6.6

3. Mechanical Properties

To obtain free-standing membrane during the exfoliation process in experiment, it is important to avoid curling or buckling. For this high in-plane stiffness of the 2D monolayer is necessary. Therefore, we now investigate the mechanical properties of the CrX_3 (X=Cl, Br, I) monolayer. The elastic moduli (listed in Table 2) are calculated by the energy vs strain method.[31] According to Born criteria,[32] a mechanically stable sheet would satisfy $C_{44}>0$, $C_{11}C_{22}-C_{12}^2> 0$. From Table 2 one find that the above criteria are

well satisfied, suggesting that they have robust mechanical stability against strain around the equilibrium positions. The Young's modulus E along an arbitrary direction θ (θ being the angle relative to the positive x direction in monolayers) can be expressed by the following equation[31]:

$$E(\theta) = \frac{C_{11}C_{22} - C_{12}^2}{C_{11}s^4 + C_{22}c^4 + \left(\frac{C_{11}C_{22} - C_{12}^2}{C_{44}} - 2C_{12}\right)c^2s^2}$$

where c=cosθ and s=sinθ. E(θ) of CrX_3 (X=Cl, Br, I) monolayer is plotted in the polar diagrams in figure 3. As can be seen, the curves of E(θ) are all close to ideal circles, demonstrating that CrX_3 (X=Cl, Br, I) monolayers are mechanically isotropic. The Young's modulus for $CrCl_3$, $CrBr_3$, CrI_3 is 31, 28, 24 N m^{-1}, respectively, which is close to the value of $MnPSe_3$ monolayer[33] and only about 7% ~9% of the in-plane stiffness for graphene (340N/m).[2] According to the elastic theory, the typical out-of-plane deformation *h* induced by gravity can be estimated as,[34]

$$\frac{h}{L} \approx \left(\frac{\rho g L}{E_{2D}}\right)^{\frac{1}{3}}$$

where ρ is the density of 2D CrX_3 (X= Cl, Br, I) as listed in Table 1. h is the size of CrX_3 (X= Cl, Br, I) flakes. Assuming L≈100 μm, we obtain *h/L* as 4.65x10^{-4}, 5.77x10^{-4}, 6.45x10^{-4} for 2D $CrCl_3$, $CrBr_3$, CrI_3, respectively. These values are of the same order of magnitude as that of graphene.[34] Thus, 2D CrX_3 (X= Cl, Br, I) can withstand its own weight and keep its free-standing planar structure.

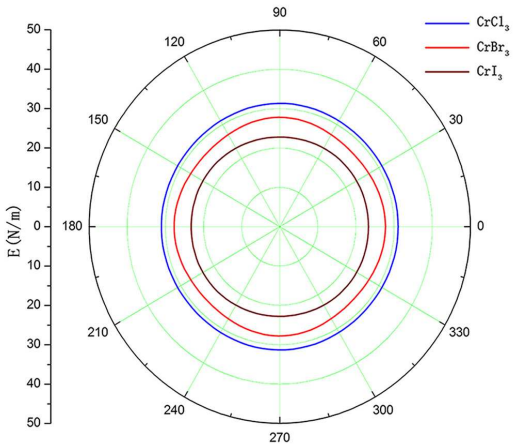

Figure 3 Polar diagrams of $E(\theta)$ of CrX_3 (X= Cl, Br, I) monolayers.

Table 2 Elastic constant (C), Young's modulus (E) of the CrX_3 (X= Cl, Br, I) monolayers

Compound	C_{11}(N m^{-1})	C_{12}	C_{22}	C_{44}	E(N m^{-1})
$CrCl_3$	33	8.07	33.3	12.34	31
$CrBr_3$	30.4	9.07	30.5	10.1	28
CrI_3	25	6.6	24.5	9.2	24

4. Electronic structures

Spin-polarized calculations are performed to find the magnetic ground state of the CrX_3 (X= Cl, Br, I) monolayer. Self-consistent calculations with different initial magnetic configurations always yield a ferromagnetic (FM) state for CrX_3 (X= Cl, Br, I) monolayer having a net magnetic moment of 6.00 μ_B in each unit cell. Moreover, the Cr ions carry most of the magnetic moment and the neighboring X (X= Cl, Br , I) ions are spin polarized antiferromagnetically. This can be seen from the isosurface of spin density ($\rho_{\downarrow} - \rho_{\uparrow}$) for FM CrX_3 (X= Cl, Br, I) monolayer in Figure 4. The corresponding numerical results are listed in the Table 3. To further confirm the most preferable magnetic coupling between the Cr ions, energies of anti-ferromagnetic (AFM) states are also calculated. Results are shown in the Figure 4, for comparison. The exchange energy defined as $E_{ex} = (E_{AFM} - E_{FM})$/unitcell for $CrCl_3$, $CrBr_3$, CrI_3 is 34, 44, 55 meV, respectively, indicating that FM state, having a lower energy, is the ground state for the CrX_3 (X= Cl, Br, I) monolayers. Moreover, the ferromagnetic coupling becomes stronger on going from the chloride to the iodide, which is owing to the different distances of neighboring Cr-Cr. The underlying mechanism of ferromagnetism can be viewed as arising from superexchange interactions between half-filled Cr t_{2g} and empty e_g states via p orbitals of X (X= Cl, Br , I) ions. This is in contrast to the antiferromagnetic direct exchange interaction of Cr t_{2g} states, which

has been studied in detail by Yaresko in chromium spinels.[35] As the neighboring Cr-Cr distance increases from $CrCl_3$ to CrI_3, direct exchange interactions ($\sim 1/d_{Cr-Cr}^5$) decrease significantly, while the indirect superexchange interaction does not change much. This finally gives rise to stronger ferromagnetic coupling in going from the chloride to the iodide. Similar result has also been reported in the recently studied $CrXTe_3$ (X = Si, Ge) nanosheets.[36]

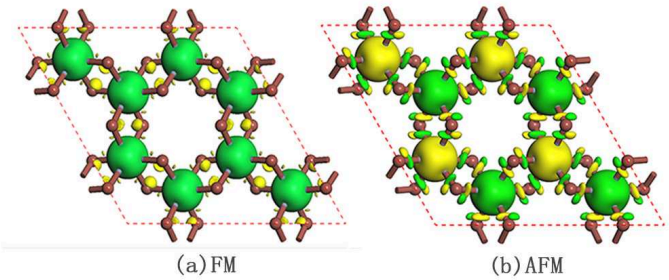

Figure 4 Spin density isosurface (isovalue: 0.03 e/Å^3) of (a) the FM and (b) AFM configurations. Green and yellow isosurfaces correspond to spin up and spin down density, respectively.

To gain an insight into the ferromagnetism of CrX_3 (X = Cl, Br, I) monolayer, spin-polarized electronic band structure and density of states (DOS) are calculated. As shown in Figure 5, all CrX_3 (X= Cl, Br, I) monolayers are semiconductors. The energy gap for $CrCl_3$, $CrBr_3$, CrI_3 is 2.28, 1.76, 1.09 eV, respectively, decreasing from the chloride to the iodide. We find that there is noticeable hybridization of Cr 3d states and halide 3p/4p/5p states in the spin up channel near the Fermi level, which further demonstrates that indirect p-d exchange interaction plays an important role in the ferromagnetic coupling of CrX_3 (X = Cl, Br, I) monolayer.

Table 3 Calculated local magnetic moments on Cr site (M_{Cr}) and X (X = Cl, Br, I) sites, total magnetic moments in a unit cell (M_U), exchange energy (E_{ex}), and band gap (E_g) .

Compound	M_{Cr}/μ_B	M_X/μ_B	M_U/μ_B	E_{ex}/meV	E_g/eV
$CrCl_3$	3.12	-0.07	6	34	2.28
$CrBr_3$	3.25	-0.1	6	44	1.76
CrI_3	3.44	-0.14	6	55	1.09

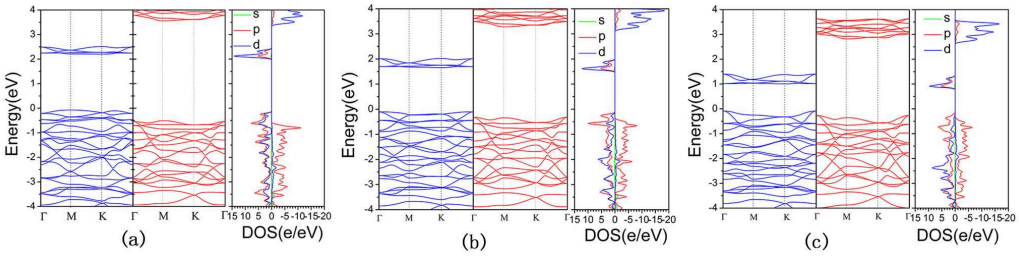

Figure 5 Band structure and corresponding density of states of (a) $CrCl_3$, (b) $CrBr_3$ and (c) CrI_3 monolayers.

5. Curie temperature

One of the important properties of ferromagnets is their Curie temperature. Using Metropolis Monte Carlo (MC) simulations[12, 15] based on the 2D Ising model we have calculated the Curie temperature of CrX_3 (X= Cl, Br, I) monolayer. According to the Ising model, the Hamiltonian of a 2D lattice can be written as $\hat{H} = -\sum_{i,j} J\hat{m}_i\hat{m}_j$, where $\hat{m}_i$ and $\hat{m}_j$ are the magnetic moments (in μ_B) at sites i and j (each chemical formula is treated as one site with the possible moment of ±3, ±1μ_B. J is the exchange parameter. For simplicity, only the nearest neighbor exchange interaction is taken into account, thus, the exchange parameter can be evaluated by $J = \frac{E_{ex}}{6m^2}$, where E_{ex} represents the exchange energy per unit cell. Therefore, J for $CrCl_3$, $CrBr_3$, CrI_3 monolayers is 0.63, 0.81, 1.02 meV, respectively. During the MC simulations, a 50x50 supercell is used to mimic the monolayer, which is found to be large enough to minimize the periodic constraints. The simulations are carried out for 10^5 loops. In each loop, the spins on all the sites in the supercell are changed according to the spin states. Through MC simulations, the variations of average magnetic moment per unit cell with respect to

temperature are calculated. The results are plotted in Figure 6. It can be seen that the magnetic moment retains high spin state in the low-temperature range and then drastically drops to near zero at a critical temperature, suggesting a thermal-induced FM-to-PM phase transition. The Curie temperature for $CrCl_3$, $CrBr_3$, and CrI_3 is estimated to be 66, 86, 107 K, respectively.

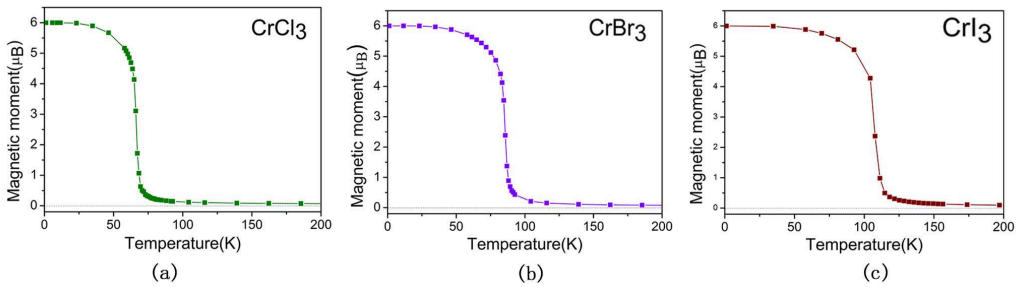

Figure 6 Variations of the average magnetic moment per unit cell with respect to temperature of (a) $CrCl_3$, (b) $CrBr_3$ and (c) CrI_3 monolayer.

6. Tuning the Curie Temperature

As the Curie temperatures of CrX_3 (X=Cl, Br, I) monolayer is far below room temperature, it is important to examine if these can be increased. We consider two strategies – applying a biaxial strain and carrier doping, which have been widely used methods to manipulate the electronic and magnetic properties of different materials.[37, 38] We first apply biaxial in-plane strain ranging from -5% to +5% and find that the local magnetic moments on Cr and X sites increase slightly with larger lattice constants while the total magnetic moment in a unit cell remains 6 μ_B. The calculated strain energies for both the FM and AFM configurations are presented in Figure 7. For the compressive biaxial strain, the exchange energy decreases significantly with the increasing strain. At the -5% biaxial strain, the exchange energy of $CrCl_3$ monolayer becomes almost zero, indicating a FM-to-PM transition, while for $CrBr_3$ (CrI_3) monolayer, it decreases to 20 (32) meV per unit cell which is about 45% (58%) of that in strain free state. The corresponding Curie temperature estimated by MC simulations decreases to 37 (62) K. For the tensile strain, only slight improvement in the exchange

energy is obtained, showing not much improvement in the Curie temperature. Thus, applying biaxial strain is not an effective strategy to enhance the FM coupling of CrX_3 (X=Cl, Br, I) monolayer.

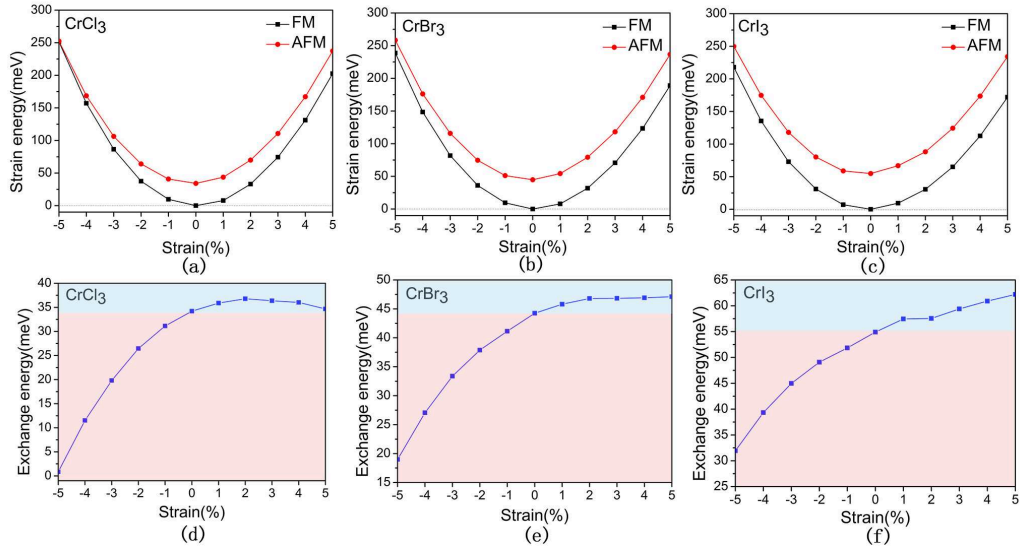

Figure 7 Strain energies of the FM and AFM configurations under biaxial strain for (a) $CrCl_3$, (b) $CrBr_3$ and (c) CrI_3 monolayer. The corresponding exchange energies ($E_{ex}=E_{AFM}-E_{FM}$) are given in (d), (e), and (f), respectively.

Next we consider tuning T_c by adding or removing electrons from CrX_3 (X=Cl, Br, I) monolayer system and using a homogeneous background charge to maintain charge neutrality. To avoid the serious distortion of the geometry, we only consider low concentration, namely up to one hole per unit cell for hole doping and up to half electron per unit cell for electron doping. We note that a carrier density modulation of $\sim 10^{15} cm^{-2}$ has already been realized in experiment using ionic liquid as gate dielectric.[39, 40] Here, the largest doping concentration is 3.10×10^{14} cm^{-2}, indicating that it is experimentally accessible. Figure 8 displays the variation of exchange energy versus carrier doping concentration. We see that both the hole and electron doping can enhance FM coupling in the CrX_3 (X= Cl, Br, I) monolayer. At same doping concentration, the increase of exchange energy by hole doping is larger than that by

electron doping. Furthermore, considering the limitation of electron doping concentration, hole doping is preferable to improve ferromagnetism of CrX_3 (X= Cl, Br, I) monolayer. At the maximum hole doping concentration considered, the calculated exchange energy of $CrCl_3$, $CrBr_3$, CrI_3 monolayer is 166.8, 160.4, and 150.4 meV/unit cell, and the T_c estimated using MC simulations is 323, 314, 293 K, respectively. These are much higher than that of previously reported 2D organic TM-Pc, inorganic MnX_2 (X=S, Se, Te)[13-15] and can be detected at room temperature. Therefore, the hole doping can significantly enhance the FM coupling of CrX_3 (X= Cl, Br, I) monolayer.

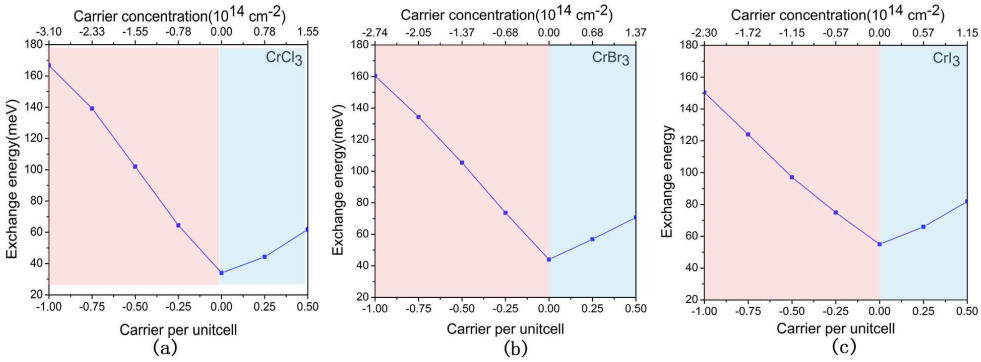

Figure 8 Exchange energies versus carrier concentration in (a) $CrCl_3$, (b) $CrBr_3$ and (c) CrI_3 monolayer. The red regions represent hole doping, while the light blue ones for electron doping.

To have a better understanding of the electronic structure of hole doped CrX_3 (X= Cl, Br, I) monolayer, we calculate the band structure and density of states with one electron removed per unitcell. Considering that the hole doping can not only lead to a redistribution of electrons but also distortion of lattice structure, we perform these calculations with full lattice relaxation. As seen from Figure 9, the hole doped CrX_3 (X= Cl, Br, I) monolayer becomes half-metallic due to the down shift of the Fermi level. In the spin up channel, the p and d bands both cross the Fermi level and electrons can be freely transported, which enhances p-d exchange interaction and gives rise to a stronger indirect ferromagnetic interaction between the

nearest-neighboring Cr ions via X (X= Cl, Br, I) bridge. Similar mechanism has also been reported in the 2D TM-Pc systems[37].

In experiment, carrier doping is usually implemented by a voltage gate with an electric field across the sheet. Therefore, we have examined the effects of such an electric field on the electronic structure of CrX_3 (X= Cl, Br, I) monolayer. Applying a rather strong electric field of 1.0 eV/Å, we calculate the band structure of CrX_3 (X= Cl, Br, I) monolayer after a full relaxation of lattice and find only slight changes. This indicates that the band structure of 2D CrX_3 (X= Cl, Br, I) is rigid against external electric fields. Therefore, it will be possible to apply voltage gate to control hole doping and then switch on/off ferromagnetism at room temperature. Thus, CrX_3 (X= Cl, Br, I) monolayer can have promising applications in spintronic devices such as spin-valve, information transport and storage between electric signals and spin signals.

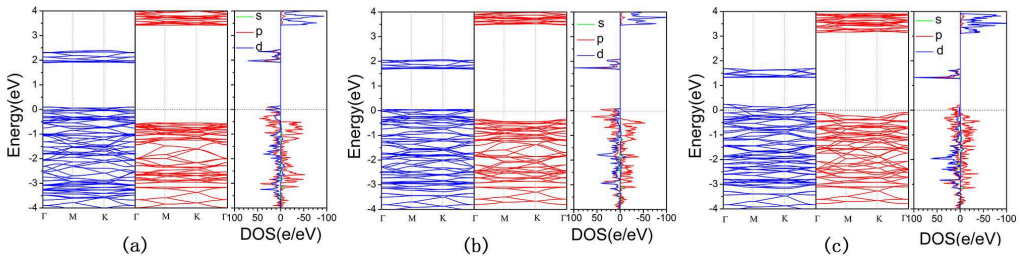

Figure 9 Band structure and corresponding density of states of (a) $CrCl_3$, (b) $CrBr_3$ and (c) CrI_3 monolayer with one hole in the unit cell.

Summary

In conclusion, we have carried out extensive first principles calculations to study the stability, electronic structure, and magnetic properties of CrX_3 (X=Cl, Br, I) monolayers and to assess the feasibility of using these for biomedical applications. The following conclusions can be drawn from our study: (1) It is possible to exfoliate CrX_3 (X=Cl, Br, I) monolayer since their cleave energies are smaller than that of graphite. (2) The in-plane stiffness of resulting 2D CrX_3 (X=Cl, Br, I) monolayers is

strong enough to withstand the curling or buckling that may be caused by gravity. Thus, these sheets can retain their planarity. (3) The Young's modulus is isotropic and much less than that of graphene. (4) All the three monolayers are semiconducting with band gaps of 2.28, 1.76, and 1.09 eV for $CrCl_3$, $CrBr_3$ and CrI_3, respectively. (5) The ground states of the monolayers are ferromagnetic similar to in-plane ferromagnetic coupling in bulk phases. The Curie temperature increases from $CrCl_3$, to $CrBr_3$ and CrI_3 due to enhanced *p-d* exchange interactions. Different from other 2D materials, strain is not effective in tuning their Curie temperature. However, hole doping can easily increase the Curie temperature, rendering these monolayers to exhibit room temperature ferromagnetism. Electric fields can be used for hole doping. Since band structures are not sensitive to external electric fields, gate voltage can be applied to significantly enhance the Curie temperature. (6) In contrast to toxic Mn-containing monolayers, the trivalent state of Cr^{3+} in CrX_3 (X=Cl, Br, I) monolayers makes these 2D materials biocompatible. Together with the displayed ferromagnetism, CrX_3 (X=Cl, Br, I) monolayers, thus, would have the potential for biological or biomedical applications such as in magnetic bio-labelling, magnetically directed drug delivery combined with hyperthermia treatment for cancer and tumors. We hope that the present study will stimulate further experimental effort on this subject.

Acknowledgment.

Q.S. acknowledges the support from the National Natural Science Foundation of China (NSFC-21173007, 11274023), from the National Grand Fundamental Research 973 Program of China (2012CB921404). PJ acknowledges support by the U.S. Department of Energy, Office of Basic Energy Sciences, Division of Materials Sciences and Engineering under Award # DE-FG02-96ER45579. YK acknowledges support by the Russian Megagrant Project No. 14.B25.31.0030 "New energy technologies and energy carriers". The authors thank the crew of the Center for Computational Materials Science, the Institute for Materials Research, Tohoku University (Japan), for their

continuous support of the HITACHI SR11000 supercomputing facility.

References

1. K. S. Novoselov, A. K. Geim, S. V. Morozov, D. Jiang, Y. Zhang, S. V. Dubonos, I. V. Grigorieva and A. A. Firsov, *Science*, 2004, **306**, 666-669.
2. C. Lee, X. Wei, J. W. Kysar and J. Hone, *Science*, 2008, **321**, 385-388.
3. W.-Q. Han, L. Wu, Y. Zhu, K. Watanabe and T. Taniguchi, *Appl Phys Lett*, 2008, **93**, 223-103.
4. K. S. Novoselov, D. Jiang, F. Schedin, T. J. Booth, V. V. Khotkevich, S. V. Morozov and A. K. Geim, *Proc Natl Acad Sci U S A*, 2005, **102**, 10451-10453.
5. J. N. Coleman, M. Lotya, A. O'Neill, S. D. Bergin, P. J. King, U. Khan, K. Young, A. Gaucher, S. De, R. J. Smith, I. V. Shvets, S. K. Arora, G. Stanton, H. Y. Kim, K. Lee, G. T. Kim, G. S. Duesberg, T. Hallam, J. J. Boland, J. J. Wang, J. F. Donegan, J. C. Grunlan, G. Moriarty, A. Shmeliov, R. J. Nicholls, J. M. Perkins, E. M. Grieveson, K. Theuwissen, D. W. McComb, P. D. Nellist and V. Nicolosi, *Science*, 2011, **331**, 568-571.
6. A. Krasheninnikov, P. Lehtinen, A. Foster, P. Pyykk 枚 and R. Nieminen, *Phys Rev Lett*, 2009, **102**, 126807.
7. A. Ramasubramaniam and D. Naveh, *Phys Rev B*, 2013, **87**, 195201.
8. Q. Wang, Q. Sun and P. Jena, *Phys Rev Lett*, 2005, **95**, 167202.
9. T. Dietl, *Nature Mater*, 2010, **9**, 965-974.
10. T. Dietl, *Science*, 2000, **287**, 1019-1022.
11. T. Hardcastle, C. Seabourne, R. Zan, R. Brydson, U. Bangert, Q. Ramasse, K. Novoselov and A. Scott, *Phys Rev B*, 2013, **87**, 195430.
12. J. Liu and Q. Sun, *Chemphyschem*, 2015, **16**, 614-620.
13. M. Kan, S. Adhikari and Q. Sun, *Phys Chem Chem Phys*, 2014, **16**, 4990-4994.
14. M. Kan, J. Zhou, Q. Sun, Y. Kawazoe and P. Jena, *J Phys Chem Lett*, 2013, **4**, 3382-3386.
15. J. Zhou and Q. Sun, *J Am Chem Soc*, 2011, **133**, 15113-15119.
16. P. Huang, G. Li, C. Chen, H. Wang, Y. Han, S. Zhang, Y. Xiao, M. Zhang, N. Liu and J. Chu, *Exp Toxicol Pathol*, 2012, **64**, 197-203.
17. D. A. Eastmond, J. T. MacGregor and R. S. Slesinski, *Crit Rev Toxicol*, 2008, **38**, 173-190.
18. S. Zhang, Y. Li, T. Zhao and Q. Wang, *Sci Rep*, 2014, **4**.
19. H. Wang, V. Eyert and U. Schwingenschlogl, *J Phys Condens Matter*, 2011, **23**, 116003.
20. L. Handy and N. Gregory, *J Am Chem Soc*, 1952, **74**, 891-893.
21. B. Morosin and A. Narath, *J Chem Phys*, 1964, **40**, 1958-1967.
22. L. J. de Jongh and A. R. Miedema, *Adv Phys*, 1974, **23**, 1-260.
23. J. P. Perdew, K. Burke and M. Ernzerhof, *Phys Rev Lett*, 1996, **77**, 3865.
24. P. E. Blöchl, *Phys Rev B*, 1994, **50**, 17953-17979.
25. G. Kresse and J. Furthmüller, *Phys Rev B*, 1996, **54**, 11169.
26. S. Grimme, J. Antony, S. Ehrlich and H. Krieg, *J Chem Phys*, 2010, **132**, 154104.

27. M. Cococcioni and S. De Gironcoli, *Phys Rev B*, 2005, **71**, 035105.

28. H. J. Kulik, M. Cococcioni, D. A. Scherlis and N. Marzari, *Phys Rev Lett*, 2006, **97**, 103001.

29. P. Giannozzi, S. Baroni, N. Bonini, M. Calandra, R. Car, C. Cavazzoni, D. Ceresoli, G. L. Chiarotti, M. Cococcioni and I. Dabo, *J Phys Condens Matter*, 2009, **21**, 395502.

30. M. A. McGuire, H. Dixit, V. R. Cooper and B. C. Sales, *Chem Mater*, 2015, **27**, 612-620.

31. E. Cadelano, P. L. Palla, S. Giordano and L. Colombo, *Phys Rev B*, 2010, **82**, 235414.

32. M. Born and K. Huang, *Dynamical theory of crystal lattices*, Oxford university press, 1998.

33. X. Li, X. Wu and J. Yang, *J Am Chem Soc*, 2014, **136**, 11065-11069.

34. T. J. Booth, P. Blake, R. R. Nair, D. Jiang, E. W. Hill, U. Bangert, A. Bleloch, M. Gass, K. S. Novoselov and M. I. Katsnelson, *Nano Lett*, 2008, **8**, 2442-2446.

35. A. Yaresko, *Phys Rev B*, 2008, **77**, 115106.

36. X. Li and J. Yang, *Journal of Materials Chemistry C*, 2014, **2**, 7071-7076.

37. J. Zhou and Q. Sun, *Nanoscale*, 2014, **6**, 328-333.

38. J. Zhou, Q. Wang, Q. Sun, Y. Kawazoe and P. Jena, *J Phys Chem Lett*, 2012, **3**, 3109-3114.

39. H. Yuan, H. Shimotani, A. Tsukazaki, A. Ohtomo, M. Kawasaki and Y. Iwasa, *Adv Funct Mater*, 2009, **19**, 1046-1053.

40. A. S. Dhoot, C. Israel, X. Moya, N. D. Mathur and R. H. Friend, *Phys Rev Lett*, 2009, **102**, 136402.